Automated Alignment and Sizing of Myocardial Stress and Rest Scans to Three-Dimensional Normal Templates Using an Image Registration Algorithm

Piotr J. Slomka, Gilbert A. Hurwitz, Janice Stephenson and Trevor Cradduck

Department of Nuclear Medicine, University of Western Ontario and Victoria Hospital, London, Ontario, Canada

To optimize the interpretation of myocardial SPECT, we developed an automated method for alignment, sizing and quantification of images using three-dimensional reference templates. **Methods:** Stress and rest reference templates were built using a hybrid three-dimensional image registration scheme based on principal-axes and simplex-minimization techniques. Normal patient studies were correlated to a common orientation, position and size. Aligned volumes were added to each other to create amalgamated templates. Separate templates were built for normal stress and rest SPECT ^{99m}Tc-sestamibi scans of 23 men and 15 women. The same algorithm was used to correlate abnormal test-patient studies with respective normal templates. The robustness of the fitting algorithm was evaluated by registering data with simulated defects and by repeated registrations after arbitrary misalignment of images. To quantify regional count distribution, 18 three-dimensional segments were outlined on the templates, and counts in the segment were evaluated for all test patients. **Results:** Our technique provided accurate and reproducible alignment of the images and compensated for varying dimensions of the myocardium by adjusting scaling parameters. The algorithm successfully registered both normal and abnormal studies. The mean registration errors caused by simulated defects were 1.5 mm for position, 1.3° for tilt and 5.3% for sizing (stress images), and 1.4 mm, 2.0° and 3.7% (rest images); these errors were below the limits of visual assessment. **Conclusion:** Automated three-dimensional image fitting to normal templates can be used for reproducible quantification of myocardial SPECT, eliminating operator-dependence of the results.

Key Words: single-photon emission computed tomography, image registration; myocardial count quantification; automated alignment; stress test

J Nucl Med 1995; 36:1115–1122

Reliable and accurate quantification of myocardial SPECT can reduce its variability and subjectivity (*1*). Existing quantification schemes (*2,3*) require user interaction, which can introduce errors in the final results (*4*). Operator-dependent steps include identifying the position of apical and basal slices, delineating the edge of the left ventricle and adjusting the orientation and translation parameters. Studies on reducing or eliminating certain user-dependent steps have been reported (*5–8*). Full automation of these procedures should result in overall improved reproducibility of the test interpretation.

In this article, a completely automated technique for the quantification of tomographic myocardial images is described. The technique is based on the concept of three-dimensional image registration. Image registration methods have been applied to correlate serial studies from the same patient (*9–11*). In contrast, we propose applying these techniques to register images of different patients to a common, normalized orientation and size. A particular problem with myocardial SPECT is the definition of the ventricular surface, which is significantly blurred due to the resolution of the camera and cardiac motion in nongated studies. Moreover, in the case of abnormal studies, the apparent edges of tracer distribution can be quite different from the actual shape of the ventricle. Therefore, volume-based image registration techniques that do not require definition of surfaces are more suitable for this application. To provide a normal reference, three-dimensional templates were built by adding normal studies after registration. Subsequently, these templates were divided into predefined regions. A relative quantification of counts in these regions could be performed on the test-images because they were registered to the same orientation as the normal templates.

METHODS

Patients

Patients were selected from a referral base of approximately 3,000 cases according to correlating angiographic and clinical information. All angiograms, as well as scintigraphic studies were ordered on clinical indications. Paired scintigraphic and angio-

Received Jun. 22, 1994; revision accepted Nov. 7, 1994.
For correspondence or reprints contact: Piotr Slomka, PhD, Victoria Hospital, Dept. of Nuclear Medicine, 375 South St., London, Ontario, Canada N6A 4G5.

graphic studies were considered for inclusion if both procedures were performed within 4 mo of each other and there was no history of Q-wave infarction. Angiograms were interpreted by a single cardiovascular radiologist unaware of the scintigraphic results. Angiographic studies were considered to be normal if there were no coronary stenoses of 50% or greater in diameter. Twenty-three male and fifteen female ^{99m}Tc-sestamibi stress-rest studies were used for the normal model. In the abnormal group, 10 male patients with single-vessel disease who had proximal stenoses of 60% or more in the proximal left anterior descending coronary artery (LAD) were selected.

Data Acquisition and Reconstruction

Images were acquired on a Siemens ZLC 7500 NCO single-head camera (Hoffman Estates, IL) with a low-energy, all-purpose collimator. Data were collected using 180° rotation, 64 × 64 matrix, 32 stops, 30 sec per stop and a circular orbit. The pixel size of the acquisition data was 6.3 mm. Center of rotation and uniformity corrections were applied to the projection images. The data were reconstructed on the Nuclear Diagnostics (Stockholm, Sweden) HERMES workstation. Two-dimensional Metz adaptive prefiltering of projection frames was applied. Filtered backprojection reconstruction was performed without applying attenuation correction. Tomograms were reconstructed with 200% zoom in the transaxial plane. Thus, the pixel size of the reconstructed images was 3.15 mm and the slice thickness was 6.3 mm.

In three cases, an extensive area of high activity in the abdomen was manually masked from the reconstructed slices by drawing regions of interest (ROIs). In other studies, it was sufficient to automatically eliminate most of the external activity by masking reconstructed volumes. Voxels outside of circular outlines (diameter equal to the matrix size) positioned perpendicular to the transverse slices were set to zero. Although this operation did not usually remove all of the abdominal activity, the registration was considerably improved. The reconstruction and masking process were the only steps requiring user interaction.

Three-Dimensional Image Registration

All registration algorithms were implemented in the C programming language using the Solaris operating environment on a Sun Microsystems, Inc. SPARC 10/512 workstation (Mountain View, CA).

Reconstructed transverse studies were correlated to each other in three-dimensions by means of an automated image registration algorithm. The algorithm had a hybrid nature. In the first step, an approximate image alignment was accomplished using a technique based on principal-axes transformation (*12,13*). This initial geometric registration was useful as a preprocessing step before a simplex minimization technique (*14*) was applied to refine the result. It was discovered that the principal-axes technique produced large angle errors in abnormal studies and could robustly estimate only scaling and translational parameters; therefore, the angle adjustment was disabled in this method.

The simplex algorithm finds the minimum of a multidimensional function; it requires only the evaluation of the function values and not the derivatives. The method starts with N + 1 estimations of the function to be minimized (where N is the dimension of the function), and through a series of steps it converges toward the smallest value. The simplex-downhill minimization algorithm was applied to iteratively improve upon the initial principal-axes image fit by independently adjusting nine transformation parameters: X scale, Y scale, Z scale, X shift, Y shift, Z shift, XY tilt, XZ tilt and YZ tilt (Fig. 1). The X, Y and Z scaling parameters were included in the search for the best fit between the two datasets to compensate for size variations between the hearts of different subjects. The measure of the difference between two image volumes represented the function value. Thus, the problem was equivalent to finding the minimum of a nine-dimensional function. Each evaluation of the function value involved a full reorientation of one dataset (32 slices 64 × 64) using three-dimensional linear interpolation (*15*). The reorientation was applied to the raw transverse data, thus avoiding the accumulation of linear interpolation errors. Other minimization algorithms (Powell and Conjugate Gradient) were also tested, but despite general recommendations of such methods (*14*), it was observed that the simplex method generally required fewer iterations to converge.

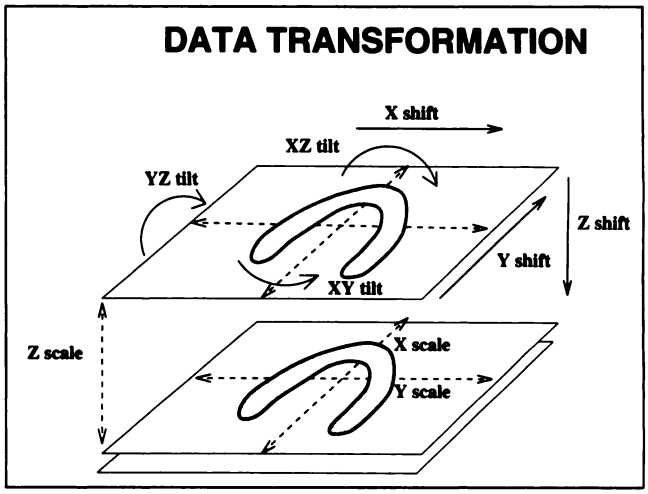

FIGURE 1. Nine linear transformation parameters used by the image registration technique to adjust orientation and size of the hearts.

Three different convergence criteria were tested for the minimization procedure: the count-difference (sum of absolute differences) as described by Hoh (*16*); the stochastic sign change (SSC), as described by Venot et al. (*17*); and the total variance of counts between two volumes (*18*). Based on the analysis of alignment errors, the count-difference method was chosen for the amalgamation of templates and the test-patient registration.

Building Composite Templates

Aligned images were sequentially added to each other, creating amalgamated datasets (Fig. 2). All datasets were registered to the templates using the same registration technique. At the end of this process, we obtained three-dimensional composite heart templates which could be viewed as tomographic scans (Fig. 3). The composite template represents an average normalized three-dimensional distribution of counts in the myocardium. Corresponding stress and rest templates were then "coregistered" to common spatial coordinates using the same image registration technique; as a result, stress and rest images of a given patient could be directly compared to each other after the registration to the templates. Separate templates for men and women were built since gender differences due to attenuation artifacts were expected. The attenuation artifact in the inferior wall was more pronounced on the male composite template (Fig. 3A). Stress and rest templates of 10 male patients with LAD disease were also built to visualize the characteristics of this defect (Fig. 4).

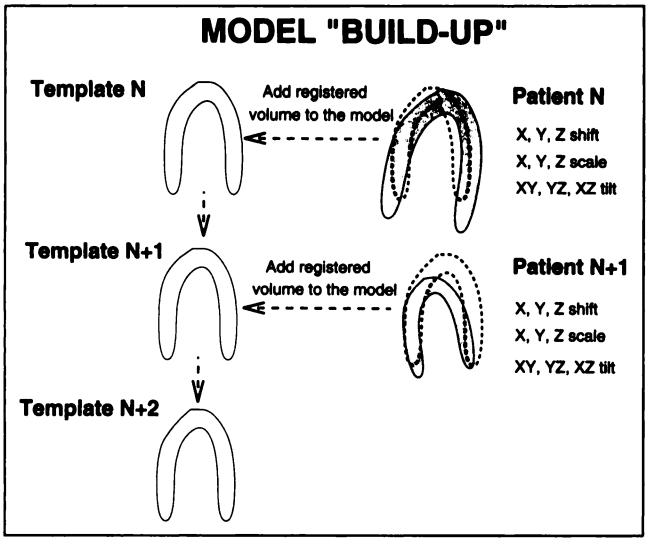

FIGURE 2. Accumulation of patient data in the normal model. Stress and rest templates were built in a cumulative fashion by registering patient studies with the composite dataset and continuously improving it by adding new registered images. Initially, two patients were selected and automatically registered to the same orientation and size. After multiplying the voxel values by the ratio of maximal counts in the 3 × 3 × 2 voxel region in the template and in the patient study, the data from these two registered volumes were added "voxel-by-voxel." Subsequently, other normal patient datasets were registered and added to the composite model.

Segmentation Scheme

To estimate regional distribution of counts, three-dimensional segmentation of the templates was performed according to a published scheme (*19*). The templates were reformatted to the short-axis orientation; six anterior slices were classified as apical, four middle slices as medial and six posterior slices as basal. The center of the ventricle was identified on short-axis slices and six symmetric segments were derived in each of the three zones (18 segments in total). The result was stored as a three-dimensional bitmap with segment codes attached to individual voxels, allowing segment identification in the registered individual patient studies.

Data Quantification

To assess the variance of count distribution in segments, all normal patients were re-registered to the composite templates and the counts for each patient in the individual segments were calculated. Images of the test-patients were normalized to the counts in the template in the same way as during the template accumulation (Fig. 2). Finally, the distribution of normalized count values expressed as a percentage of counts in the templates was derived.

The same method was used to register abnormal test-patient scans to the stress-rest template pairs. Counts in each segment were calculated and normalized to the averaged maximum. In a preliminary assessment of automated detection of perfusion defects, we used this quantification technique in a group of 10 patients with LAD lesions. The results were then compared to the count distribution in normal templates. In addition, the difference between stress and rest counts in individual segments was assessed. The count-difference could be readily obtained by subtracting the stress and rest images since their respective templates were registered to each other. Finally the segments were classified as abnormal if the normalized counts were at least 2 s.d.s below the template counts in corresponding segments.

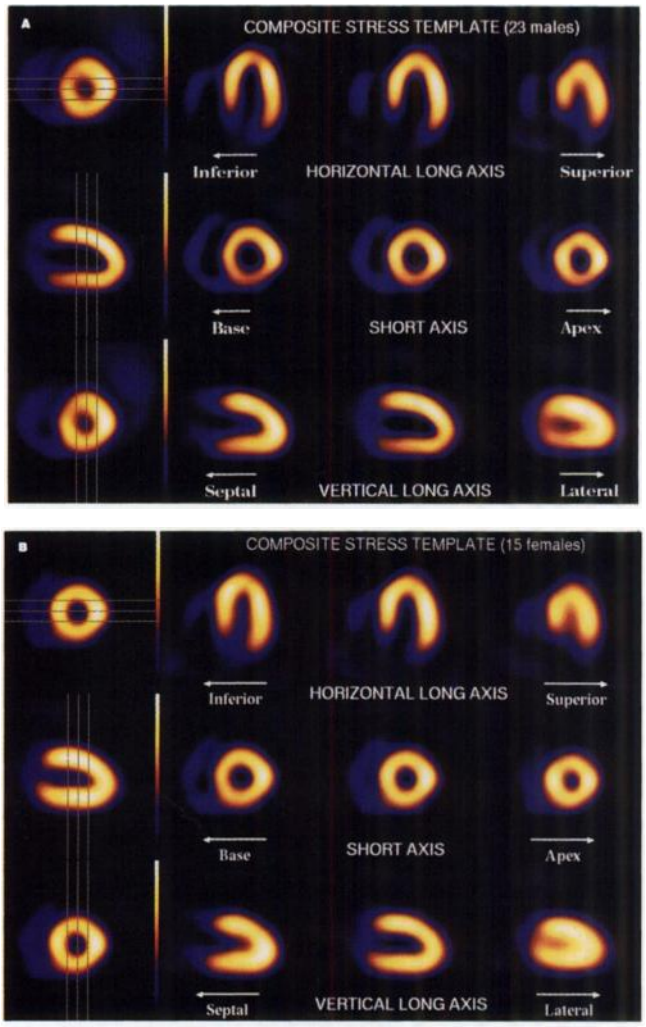

FIGURE 3. (A) Male and (B) female normal composite stress templates. The smaller female template was resized to the male template dimensions.

Visual Assessment of Registration Accuracy

The result of each automated alignment was carefully assessed by an experienced nuclear medicine technologist. Several visual presentation techniques were utilized to verify the registered image accuracy: (1) image overlay of the template image and aligned patient images; (2) synchronized cursors indicating corresponding positions on the registered image and the normal template; (3) a roving window display technique (Fig. 5); (4) subtracted display revealing registration discrepancies between the normal template and the patient image. The quality of the fit was examined on all image slices in different orientations.

Quantitative Assessment of the Fitting Algorithm

To quantitatively assess the robustness of the fitting algorithm, we analyzed the effect of simulated defects and the effect of the initial alignment on registration accuracy. The statistical significance of the results was determined using analysis of variance of repeated measures and follow-up comparisons of specific means by the Newman-Keuls test (*20*).

To estimate the accuracy of the algorithm in the processing of abnormal data, 16 simulated defects were generated on images from one normal patient. The simulated defects were introduced at various locations in the left ventricle on stress and rest images;

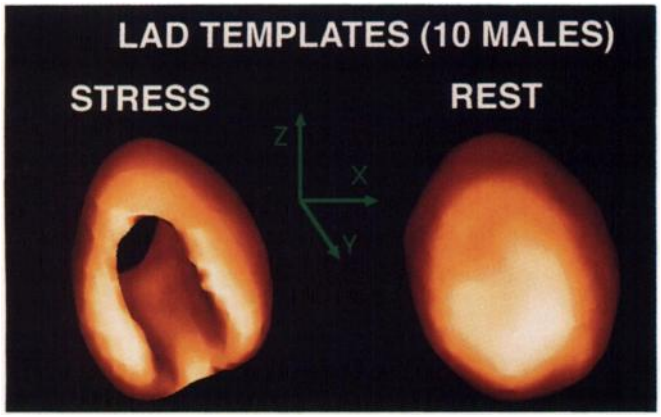

FIGURE 4. Three-dimensional surface-shaded display of stress (left) and rest templates (right) in men with abnormal left anterior descending coronary arteries.

their size varied between 20% and 40% of the myocardial volume. Simulated defects had voxels values set to zero. Images with simulated defects were then arbitrarily misaligned (angles and shifts) and subsequently registered to the normal templates. Registrations of images with simulated defects were performed separately for three different convergence criteria. Registration parameters from the original unmodified study provided an absolute reference to which the registrations of images with simulated defects were compared. The registration error for each transformation parameter was defined as the absolute change related to the introduction of the defect.

The reproducibility of the spatial registration of the count-difference method was assessed in a quantitative fashion. Patient studies were misaligned using 20 different combinations of position and tilt parameters and subsequently registered to the normal templates; the angles were changed between $-20°$ and $20°$ and shifts between -8 and 8 pixels. This task was performed on 10 normal and 10 abnormal stress-rest datasets, resulting in 800 registrations. The reproducibility error for each transformation parameter, defined as the maximum difference from the mean value for 20 misalignments, was estimated individually for each patient study.

The effect of the worst misalignment errors on the count distribution in 18 segments was also assessed. The two patient studies (one normal, one abnormal) with the highest errors in the registration reproducibility test were selected for this test. Count values were derived from each segment of both stress and rest

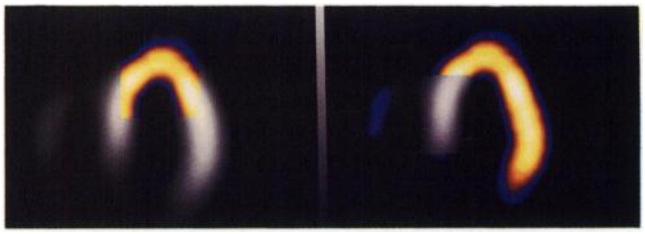

FIGURE 5. Roving window technique for visual assessment of image registration. The grey-scale image represents the template; the color image represents the patient data. A patient image subwindow can be displayed and interactively moved on the template image (left). A template subwindow can be displayed and moved on the patient image (right).

FIGURE 6. Midventricular slices of a stress study with a severe LAD defect (color) overlaid on the model data (grey scale). Horizontal long-axis is shown on the left, short-axis in the middle and vertical long-axis on the right.

datasets after the images were registered with 20 different initial orientations. Subsequently, coefficients of variation of the alignment results were determined.

RESULTS

Calculation Time

The mean number of iterations required by the simplex-downhill algorithm for each patient fit was 275; each iteration took about 1 sec. Thus, the total time for finding the minimum was approximately 4 min for each registration. The time involved in the initial principal-axes reorientation was roughly equivalent to one iteration of the simplex algorithm.

Visual Assessment of the Registration

A misregistration of size (subjectively assessed as smaller than 10%) was visually detected only in one case. It occurred due to a significant amount of liver activity remaining in the image despite the masking procedure. After removing this external activity, the algorithm properly registered the images. Discrepancies between the patient data and corresponding templates were observed when the principal-axes registration was performed without further iterative minimization. The quality of this geometric registration was worse with abnormal scans or in the presence of remaining external activity. When the principal-axes method was combined with the simplex-minimization, errors could not be detected visually. Even in patients with abnormal hearts, the registration algorithm properly reoriented the images (Fig. 6).

Assessment of Simulated-Defects Registration Errors

Registration errors for different convergence criteria due to simulated defects are shown in Table 1. Overall, fitting errors were significantly lower for the count-difference method than for the other two methods on stress images ($p \leq 0.0002$) and rest images ($p \leq 0.003$). Specifically, errors for several of the scaling and tilt parameters were significantly lower in comparison to the SSC and variance methods (Table 1). Based on these results, the count-difference was chosen for the subsequent test of fitting reproducibility and for final patient registration. When comparing fitting parameters to each other for the count-difference method, it was found that Y scaling errors were significantly larger than X and Z scaling errors ($p \leq 0.0005$) for stress images and significantly larger than Z scaling errors ($p = 0.008$) for rest images. For the count-difference

TABLE 1
Mean Registration Errors for Three Different Convergence Criteria in the Simulated Defect Experiment

	Count difference		Stochastic sign change		Variance	
	Stress	Rest	Stress	Rest	Stress	Rest
X shift (mm)	1.2	1.2	3.1	2.0	3.2	3.6
Y shift (mm)	1.5	1.4	2.7	1.6	4.4	4.4
Z shift (mm)	0.8	0.9	1.4	0.9	1.7	1.9
X scale (%)	3.0	3.2	4.7	6.3	9.7*	11.1*
Y scale (%)	5.3	3.7	4.2	2.0	11.8*	10.5*
Z scale (%)	1.5	1.9	7.1*	4.8	5.8	4.9
XY tilt (deg)	1.3	1.4	5.9	2.6	5.2	3.1
XZ tilt (deg)	0.8	1.3	7.9*	4.3	2.4	3.5
YZ tilt (deg)	1.3	2.0	7.6*	6.2	1.8	2.9

*Significantly worse than the count-difference method $p \leq 0.007$.
n = 16 simulated defects at various locations of the myocardium.

method, the overall differences between stress and rest with respect to fitting errors were not significant ($p = 0.5$).

Assessment of Registration Reproducibility

Errors of the transformation parameters for normal and abnormal (LAD defect) patients are shown in Table 2. There was no significant difference between fitting of normal and abnormal studies ($p = 0.3$), but fitting of stress studies was better than rest studies ($p \leq 0.0007$). Specifically, the fitting of abnormal stress studies was more reproducible than in the other three groups ($p \leq 0.002$). For normal stress and rest studies, the errors of the scaling in the Y direction were significantly worse than errors in the X and Z direction ($p \leq 0.0002$) and tilt error in the XZ direction was significantly worse than the XY tilt error ($p = 0.05$). For abnormal stress and rest studies the scaling error in the Y direction was significantly worse than in the X or Z direction ($p \leq 0.05$).

The hybrid nature of the algorithm was the reason for good convergence, even when the images were initially grossly misaligned. The application of a fast, but less accurate principal-axes method to estimate initial position and scaling decreased the number of iterations for the more precise simplex algorithm; it also improved the robustness of the iterative algorithm. We experienced difficulties in simplex algorithm convergence when the images were significantly misaligned and when the initial principal-axes technique was not used.

TABLE 2
Reproducibility of Registration after Arbitrary Misalignments*

	Normal studies		Abnormal studies	
	Stress	Rest	Stress	Rest
X shift (mm)	0.2 ± 0.1	0.4 ± 0.3	0.4 ± 0.3	0.3 ± 0.2
Y shift (mm)	0.7 ± 0.5	0.8 ± 0.4	0.7 ± 0.6	0.6 ± 0.4
Z shift (mm)	0.3 ± 0.1	0.5 ± 0.3	0.2 ± 0.3	0.4 ± 0.3
X scale (%)	1.2 ± 0.4	1.5 ± 0.6	0.9 ± 1.0	1.8 ± 0.9
Y scale (%)	3.8 ± 1.9	3.6 ± 2.7	2.0 ± 2.0	3.0 ± 1.7
Z scale (%)	2.0 ± 1.3	2.2 ± 0.7	1.2 ± 1.5	2.3 ± 1.3
XY tilt (deg)	1.1 ± 0.5	1.1 ± 0.7	0.7 ± 0.8	1.1 ± 0.7
XZ tilt (deg)	2.1 ± 1.3	2.1 ± 1.2	0.9 ± 1.1	2.8 ± 1.5
YZ tilt (deg)	1.4 ± 0.8	2.1 ± 1.6	0.9 ± 1.0	2.0 ± 1.0

*Mean errors ± s.d. of transformation parameters for the count-difference method.
s.d. = one standard deviation; n = 10 datasets (each misaligned 20 times).

The results in Table 3 describe the influence of the registration error on the final quantification results in individual segments. One normal and one abnormal patient study are presented, for which the largest errors were observed in the registration reproducibility test (Table 2).

Data Analysis of Test Patient Results

In a preliminary assessment of the potential diagnostic use of our automated method, the count distribution was evaluated for individual segments in normal patients and in patients with angiographically proven LAD disease. The variation of counts in segments in the normal male stress and rest groups is shown in Figure 7. The classification results of abnormal patients are presented in Figure 8. All LAD patients had some abnormal segments based on the 2 standard deviation criteria. In most cases, the abnormality was detected in the antero-septal regions of apical and mid-ventricular zones. Differences between the stress and rest provided well defined results.

Difference images created by subtraction from the normal stress and rest templates can illustrate deviations from the normal distribution without using arbitrary segments (Fig. 9). Such images can be used to visualize the extent and location of perfusion defects. The differences between defects at stress and rest provide an estimate of ischemia. The stress template built from the group of LAD patients clearly showed the characteristics of this defect (Fig. 4). Similar templates could be built for other groups falling into specific diagnostic categories of angiographically defined disease; they could be used to estimate zones of expected hypoperfusion on the templates.

DISCUSSION

Image Registration Method

The template-based requirement of our registration method, as compared to the registration of serial data from one patient, is the need to independently adjust three scaling parameters, which are not known a priori. Scaling parameters play an important role because the dimensions of the myocardium vary between patients. Combining three independent scaling parameters (X, Y, Z) into one or two factors would decrease the number of iterations. Nevertheless, because of the individual size variations in each dimension, it was important to include these factors as individual components in the search for the minimum. For example, dilated ventricles (two cases in the LAD group) had a roughly spherical shape; the algorithm compensated for this effect by adjusting the X-scaling parameter which

TABLE 3
Effect of Alignment Errors on Segmental Count Distribution in Two Patients (One Normal, One Abnormal) with the Highest Registration Errors in the Reproducibility Test

Worst segments	Coefficient of variation*	
	Stress	Rest
Normal patient		
Basal high lateral	3.9%	3.0%
Basal anteroseptal	3.0%	2.3%
Basal inferolateral	2.6%	2.0%
Basal anterior	2.3%	1.8%
Others	≤2.0%	≤2.0%
Abnormal patient		
Apical inferoseptal	2.4%	1.8%
Apical anteroseptal	2.2%	1.9%
Apical inferior	2.2%	2.8%
Apical high lateral	2.1%	1.5%
Basal high lateral	1.1%	2.6%
Basal anterior	0.8%	2.5%
Others	≤2.0%	≤2.0%

*Variation of relative count values in segments; n = 20 misalignments and registrations.

changed the patient images to an approximately ellipsoidal shape of the normal template. Scaling parameters may also be used to quantitatively estimate the volume of the ventricle, which could have potential diagnostic value (*21,22*).

Registering differently shaped hearts to common templates raises questions of the validity of the linear transformations. It should be possible, for example, to apply nonlinear scaling, or "warping" techniques that adjust more than nine parameters to compensate for different shapes (*23*). Such a method was recently proposed by Houston et al. for the registration of brain studies (*24*). The disadvantage, however, would be the distortion of relative count distribution in the myocardium; therefore, it would be difficult to compare such techniques with established quantification schemes (*3*). The use of linear scaling preserves the relative count ratios and defect sizes; therefore, the quantification of data is more straightforward. Despite amalgamating a number of patients using linear transformations, the composite images retain the essential characteristics of myocardial scans, and there is no significant loss of resolution (Fig. 3).

The most noticeable characteristics of the composite templates were the low noise and background levels and the slightly smoothed and "blurred" appearance of the images. The smooth appearance could be attributed to a much higher number of counts in the templates than in single-patient images. Blurred edges were most likely caused by nonlinear differences in ventricular shapes. Due to the low resolution of the original images, however, these differences do not seem to significantly affect the resolution of the composite images. The relatively good quality of template images can be explained by the lack of fine details in the original images, which are blurred by cardiac motion and are generally of low resolution. The myocardial walls on the female template are thicker, perhaps due to relatively lower resolution of generally smaller hearts.

The count-difference convergence criterion provided better results than SSC or the variance method (Table 1). Hoh et al. (*16*) did not find any significant difference between the SSC and count-difference method, but they used the algorithm to register serial studies of the same patient and did not search for scaling parameters.

Although the registration algorithm requires a relatively long computing time, especially during iterative reorienting of the data, several techniques can be utilized to improve

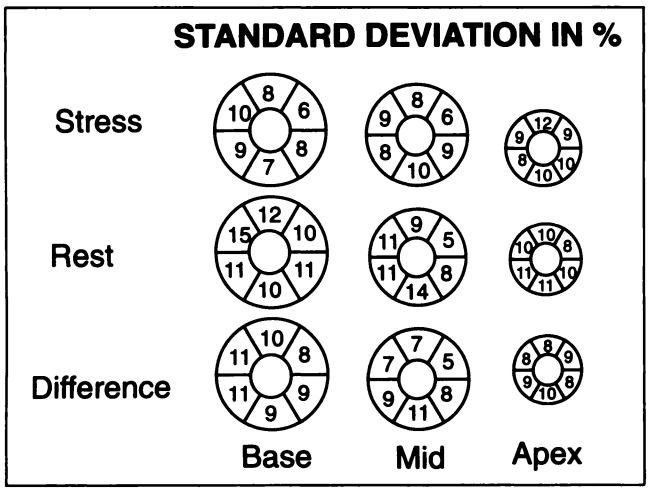

FIGURE 7. Standard deviations of relative count distribution in each segment for stress, rest and the difference between stress and rest in the normal male group (n = 23). Orientation is identical to the short-axis slice orientation in Figure 3. Rest segments had generally higher standard deviations than corresponding stress segments. The stress-rest subtraction images had smaller variation in most segments than the stress and rest images assessed separately. The standard deviation was smallest in the apical, medial and basal high-lateral and inferior-lateral segments and highest in the inferior segments.

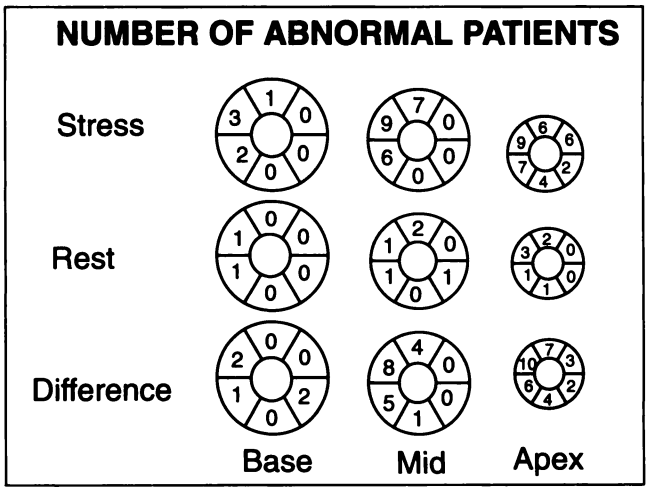

FIGURE 8. Abnormal segments in the LAD group of 10 male patients. The number of patients with abnormal results (more than 2 s.d.s below the mean) are shown for each segment individually.

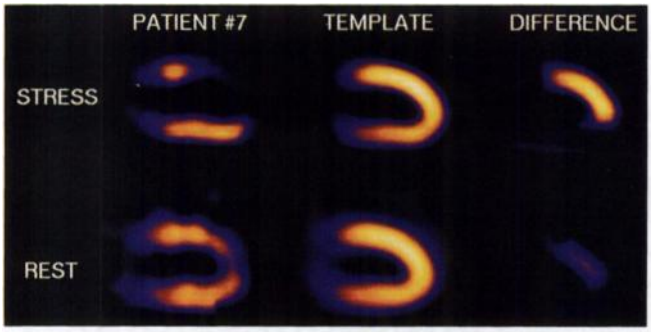

FIGURE 9. Subtraction of the abnormal (LAD) stress (top) and rest (bottom) patient images (left) from the normal model (middle). Subtracted images (right) visualize the extent of the defect on stress and rest scans.

its speed for routine clinical use. Some of the methods for fast image reorientation are described by Hoh et al. (*16*). The relatively small matrix size and small number of slices in myocardial SPECT studies allowed the implementation of computationally intensive algorithms on a standard, mid-range computer. These algorithms would be currently impractical for larger matrix sizes due to lengthy computation times. The principal-axes technique is fast due to its analytical character but the accuracy is unsatisfactory for this application. Nevertheless, its use for initial image alignment increases the robustness of the algorithm and reduces the number of subsequent iterations.

Alignment Accuracy

The accuracy of automated registration (Tables 1, 2) compared to the pixel size (6.3 mm) and the resolution of the scan (generally above 15 mm) is encouraging. The scaling error of 5% or the angular error of 2° translates approximately to 3-mm displacement in the apex of an average heart. The lower accuracy of scaling in the Y direction (Tables 1, 2) and tilting in the XZ direction (Table 2) may be attributed to the shape of the ventricle; data transformation in these directions corresponds to relatively smaller changes in the count-difference criteria. The registration errors in our automated technique are below the limit of visual assessment. Other methods have been previously designed to automatically adjust selected orientation parameters of the left ventricle (*5–8*). The advantage of our technique is that all parameters are considered, including three independent scalings and three angles.

An objective measure of the algorithm performance with abnormal data was provided by the simulated-defect registration (Table 1). The results showed that alignment was accurate even when a considerable part of the myocardium was missing. The method is robust despite the presence of defects because the algorithm searches for the relative minimum of the count-difference. Although the simulated defects increased the count difference between patient image and the template, the relative minimum was found for the transformation parameters which approximated the original data registration. Registration errors in the simulated-defect test may have been amplified due to the fact that the introduced lesions did not contain any counts. In extreme cases, when most of the myocardium is missing, the registration may produce larger errors; in these situations, however, an accurate quantification is usually not critical. The clinical importance of accurate registration may be greater for mildly abnormal, borderline cases.

Both normal and abnormal images could be fitted with very good reproducibility. The fitting of abnormal stress studies was more reproducible than fitting of normal studies probably because of a better-defined minimum of the count-difference between the template and abnormal studies (Table 2). Worse reproducibility of rest fitting (Table 2) can be attributed to lower counts in the rest images. Compared to the traditional manual adjustment used in the bull's-eye quantification program (*3*), the error of one slice in the selection of basal or apical limits would be equivalent to an 8% scaling error (assuming 12 short-axis slices). Small errors caused by the misalignment indicate that the technique is relatively insensitive to the initial position and orientation of the reconstruction. Therefore, registration can be applied to raw transverse images without prior manual alignment and true short-axis, horizontal long-axis or vertical long-axis slices can be automatically derived. The effect of a random misalignment registration error on the quantification results is smaller than the variation in normal count distribution (Table 3, Fig. 7).

Image Quantification

The division of the templates into segments is one example of quantification possibilities; the described method could be used with different region definitions. Other arrangements of segments for myocardial perfusion quantification were proposed by Maublant et al. (*25*) for SPECT and by Kotzerke et al. (*26*) for PET studies. Another application of the method could be processing of the images subtracted from the normal distribution. For example, it should be possible to estimate the abnormal region location and size by processing the three-dimensional images subtracted from the template (Fig. 9). In a preliminary study, we have developed a region-growing technique to estimate defect parameters on subtracted images normalized by the standard deviation values for normal studies calculated at each voxel (*27*). This approach would eliminate the need for the segmentation scheme. It is also conceivable to combine our method with the bull's-eye quantification scheme by applying the registration algorithm as a preprocessing step. Although the described method has been evaluated for myocardial stress and rest perfusion images, it has more general applications. In particular, the quantification of HMPAO brain scans or lung ventilation/perfusion SPECT scans could be based on a similar scheme.

CONCLUSION

The use of three-dimensional templates has potential advantages in comparison to the popular bull's-eye display (*3*). It can provide more natural three-dimensional data visualization and representation, which is not constrained

to predefined geometrical shapes. Furthermore, the voxel-based three-dimensional character of our approach may facilitate the estimation of defect volume by comparing the templates and test-data on a voxel level. In comparison, on the polar map it is possible to estimate only the area, which subsequently can be related to volume (*4*). Accurate, automated alignment of the data with our registration method could provide more objective results than manual methods of reorienting and repositioning of the ventricle. During three-dimensional image reorientation, the scaling, sizing and tilt parameters are dependent on each other and it is difficult to adjust one parameter accurately without influencing the optimal position of the others; the interactive methods usually rely on changing these parameters sequentially. In contrast, our method optimizes all position, size and orientation alignment parameters simultaneously.

ACKNOWLEDGMENTS

The authors thank Dr. Frank Prato for useful discussions and Ms. Soraya Ali for help in preparing the manuscript.

REFERENCES

1. Garvin AA, Cullom JS, Garcia EV. Myocardial perfusion imaging using single-photon emission computed tomography. *Am J Cardiac Imag* 1994;8: 189–198.
2. Van Train KF, Berman DS, Garcia EV, et al. Quantitative analysis of stress thallium-201 myocardial scintigrams: a multicenter trial. *J Nucl Med* 1986; 27:17–25.
3. Garcia EV, Cooke CD, Van Train KF, et al. Technical aspects of myocardial SPECT imaging with technetium-99m-sestamibi. *Am J Cardiol* 1990;66: 23E–31E.
4. Garcia EV. Quantitative myocardial perfusion single-photon emission computed tomographic imaging: quo vadis? (Where do we go from here?). *J Nucl Cardiol* 1994;1:83–93.
5. Ezekiel A, Van Train KF, Berman D, Silagan D, Maddahi J, Garcia EV. Automatic determination of quantification parameters from Tc-sestamibi myocardial tomograms. In: *Computers in cardiology*. New York: IEEE; 1991:237–240.
6. Mullick R, Ezquerra NF, Garcia EV, Cooke CD, Folks RD. Three-dimensional visualization of pose determination: application to SPECT imaging. *Visualization Biomed Computing Proc SPIE* 1992;1808:225–234.
7. He Z, Maublant JC, Cauvin JC, Veyre A. Reorientation of the left ventricular long-axis on myocardial transaxial tomograms by a linear fitting method. *J Nucl Med* 1991;32:1794–1800.
8. Cauvin JC, Boire JY, Maublant JC, Bonny JM, Zanca M, Veyre A. Automated detection of the left ventricular myocardium long axis and center in thallium-201 single photon emission computed tomography. *Eur J Nucl Med* 1992;19:1032–1037.
9. Pelizzari CA, Chen GTY, Spelbring DR, Weichselbaum R, Chen CT. Accurate three-dimensional registration of CT, PET and/or MR images of the brain. *J Comput Assist Tomogr* 1989;13:20–26.
10. Junck L, Moen JG, Hutchins GD, Brown MB, Kuhl DE. Correlation methods for the centering, rotation and alignment of functional brain images. *J Nucl Med* 1990;31:1220–1226.
11. Turkington TG, Jaszczak RJ, Pelizzari CA, et al. Accuracy of registration of PET, SPECT and MR images and MR images of a brain phantom. *J Nucl Med* 1993;34:1587–1594.
12. Faber TL, Stokely EM. Orientation of three-dimensional structures in medical images. *IEEE Trans Pattern Anal Machine Intell* 1988;10:376–380.
13. Alpert NM, Bradshaw JF, Kennedy D, Correia JA. The principal axes transformation—a method for image registration. *J Nucl Med* 1990;31:626–633.
14. Press WH, Teukolsky SA, Vetterling WT, Flannery BP. *Numerical recipes in C*, 2nd edition. New York: Cambridge University Press; 1992;408–412.
15. Press WH, Teukolsky SA, Vetterling WT, Flannery BP. *Numerical recipes in C*, 2nd edition. New York: Cambridge University Press; 1992;123–128.
16. Hoh CK, Dahlbom M, Harris G, et al. Automated iterative three-dimensional registration of positron emission tomography images. *J Nucl Med* 1993;34:2009–2018.
17. Venot A, Liehn JC, Lebruchec JF, Roucayrol JC. Automated comparison of scintigraphic images. *J Nucl Med* 1987;27:1337–1342.
18. Russ JC. *The image processing handbook*. Boca Raton, FL: CRC Press; 1992;240.
19. Berman D, Kiat H, Van Train KF, Garcia EV, Friedman J, Maddahi J. Technetium-99m-sestamibi in the assessment of chronic coronary artery disease. *Semin Nucl Med* 1991;21:190–212.
20. Myers JL. *Fundamentals of experimental design*. Boston: Allyn and Bacon Inc.; 1979;162–198.
21. Lamas GA, Pfeffer MA. Left ventricular remodeling after acute myocardial infarction: clinical course and beneficial effects of angiotensin-converting enzyme inhibition. *Am Heart J* 1991;121:1194–1202.
22. Akinboboye OO, Haines FA, Atkins HL, Oster ZH, Brown EJ. Assessment of left ventricular enlargement from planar thallium-201 images. *Am Heart J* 1994;127:148–51.
23. Gonzales RC, Woods RE. *Digital image processing*. Reading MA: Addison-Wesley Publishing Company; 1992;298.
24. Houston AS, Kemp PM, Macleod MA. A method for assessing the significance of abnormalities in HMPAO brain SPECT images. *J Nucl Med* 1994;35:239–244.
25. Maublant JC, Peycelon P, Kwiatkowski F, et al. Comparison between 180° and 360°, data collection in technetium-99m MIBI SPECT of the myocardium. *J Nucl Med* 1989;30:295–300.
26. Kotzerke J, Hicks RJ, Wolfe E, et al. Three-dimensional assessment of myocardial oxidative metabolism: a new approach for regional determination of PET-derived carbon-11-acetate kinetics. *J Nucl Med* 1990;31:1876–1893.
27. Slomka PJ, Hurwitz GA, St Clement G, Stephenson JA. Three-dimensional demarcation of coronary artery perfusion zones: towards automated interpretation of myocardial tomography [Abstract]. *J Nucl Cardiol* 1955; 2:S37.